Broadband Single-Shot Electron Spectrometer for GeV-Class Laser Plasma Based Accelerators

K. Nakamura,* W. Wan, N. Ybarrolaza, D. Syversrud, J. Wallig, and W. P. Leemans

Lawrence Berkeley National Laboratory,

University of California, Berkeley, CA 94720, USA

(Dated: October 26, 2007)

Abstract

Laser-plasma-based accelerators can provide electrons over a broad energy range and/or with large momentum spread. The electron beam energy distribution can be controlled via accurate control of laser and plasma properties, and beams with energies ranging from $\simeq$0.5 to 1000 MeV have been observed. Measuring these energy distributions in a single shot requires the use of a diagnostic with large momentum acceptance and, ideally, sufficient resolution to accurately measure energy spread in the case of narrow energy spread. Such a broadband single-shot electron magnetic spectrometer for GeV-class laser-plasma-based accelerators has been developed at Lawrence Berkeley National Laboratory. A detailed description of the hardware and the design concept is presented, as well as a performance evaluation of the spectrometer. The spectrometer covered electron beam energies raging from 0.01 to 1.1 GeV in a single shot, and enabled the simultaneous measurement of the laser properties at the exit of the accelerator through the use of a sufficiently large pole gap. Based on measured field maps and 3rd-order transport analysis, a few percent-level resolution and determination of the absolute energy were achieved over the entire energy range. Laser-plasma-based accelerator experiments demonstrated the capability of the spectrometer as a diagnostic and its suitability for such a broadband electron source.

PACS numbers:

I. INTRODUCTION

A charged particle spectrometer[1] is one of the critical diagnostics for any particle accelerator. Laser-driven plasma wakefield accelerators (LWFA)[2,3] have shown significant progress over the last decade, and have attracted considerable interest as the next generation linear accelerators. For the present generation LWFAs, requirements placed on the electron spectrometer (ESM) are somewhat different from those for conventional accelerators. A broad momentum acceptance with high resolution is critical. LWFAs can operate in a regime where beams with large relative energy spread $\delta E/E$ are generated[4–7], or, as has recently been shown, produce narrow ($< 10\%$) $\delta E/E$ beams[8–13], where E is the electron kinetic energy. In addition, by controlling laser and plasma conditions, it has been shown that narrow energy spread beams can be generated with energies ranging from 0.5 GeV - 1 GeV[14,15]. To elucidate the mechanisms behinds those regimes hence requires the use of a ESM with broad momentum acceptance. Although the required momentum resolution for LWFA could be somewhat relaxed compared to those for conventional accelerators, it should perform at a few percent level resolution to accurately measure the energy spread of the present generation LWFA beams.

Most spectrometer implementations use a dipole magnet as a dispersive element and a collimator to control the instrumental resolution. To detect the relativistic electron, a variety of detectors have been employed: surface barrier detectors[4,5,16], cloud chambers[16], thermoluminescent dosimeters (TLD)[17], scintillating fibers[18,19], scintilators with photomultipliers[6,7], imaging plates (IP)[8,11,12,20], and scintillating screens, mostly Gadox ($Gd_2O_2S:Tb$)[21] with films[4] or cameras (scint.-camera)[6,13,15,16,22]. IP and scint.-camera detectors are now widely used for their capability of imaging, and hence can provide detailed information of the spatial properties. Due to the capability of accumulative measurements, IP has an advantage in sensitivity, while scint.-camera based system could allow a high repetition-rate operation.

Recently, production of up to 1 GeV electron beams (e-beam) via a capillary discharge guided (CDG-) LWFA has been demonstrated by LOASIS Group at Lawrence Berkeley National Laboratory (LBNL)[14,15]. When the CDG-LWFA experiments were designed, the decision was made to develop a magnet-based ESM with as large a momentum acceptance as possible and capable of measuring e-beams of order GeV. In the CDG-LWFA accelerator concept, guiding of an intense laser was critical for operation, therefore simultaneous mea-

surement of laser output mode and e-beam properties was essential. In order to realize the simultaneous measurement, the laser beam had to be separated from the e-beam without significant distortion, and, to accommodate such a broad energy spectrum without having a large system, the ESM magnetic field had to be reasonably strong ($\geq$ 1 T). In addition, the design needed to provide sufficient angular acceptance to address the e-beam angular properties, as well as single-shot evaluation capability with high repetition rate for statistical analysis. In this paper, the ESM design concept and the description of the hardware are presented in Section II, followed by the performance evaluation of the ESM in Section III. Section IV presents experimental results, and a summary is given in Section V.

II. SPECTROMETER DESIGN

The electron magnetic spectrometer utilized a water-cooled round dipole electro-magnet Varian 4012A, which had a 65 mm gap and was powered by a Glassman SH3R2.7 power supply. Since it was originally used for magnetic resonance experiments[23], the field homogeneity in the flat region was very high ($< 1\%$ variations). The magnetic field was measured by a Hall probe along the mid-plane[1], and the effective radius, defined by $R_{eff} = [\int_0^\infty B_x(r)dr]/B_x(0)$, was found to be 195 mm with peak field $B_x(0) = 1.25$ T. The Hall probe was installed permanently to measure the peak magnetic filed strength $B_x(0)$ for each shot directly rather than deducing the peak field from the applied magnet current, which could lead wrong estimates due to the hysteresis. The magnet deflected the electrons vertically downward onto two scintillating screens (LANEX Fast Back) mounted on the exit flanges of the vacuum chamber. Four synchronously triggered 12-bit charge-coupled device (CCD) cameras imaged a 75 cm long (bottom) and a 45 cm long (forward) screens, allowing simultaneous single shot measurement of electrons from 0.01 GeV to 0.14 GeV (bottom) and 0.17 GeV to 1.1 GeV (forward) with a magnetic field of 1.25 T. Spatial resolutions of those CCD cameras were measured to be $0.6 - 1$ mm for the forward screen and $\simeq 2.5$ mm for the bottom screen (see Fig. 2). Stray laser light was blocked by $\simeq 40\mu$m thick aluminum foil on the back of the screens. In addition, bandpass filters (central wavelength 550 nm, width 70 nm full-width half-maximum (FWHM)) were installed in front of each CCD camera to separate green fluorescent light from the intense infrared laser light. To avoid electrons from hitting the CCD cameras directly, first-surface mirrors were used at 45° following the exit flanges, which

separated fluorescent light from the electrons. The total number of electrons was obtained from the intensity on the phosphor screen, that was cross-calibrated against an integrating current transformer.

The imaging properties of the spectrometer were determined via the edge focusing. The displacement of the dipole magnet center with respect to the laser propagation axis was carefully chosen to provide the necessary edge focusing. Since converging powers in the dispersive (vertical, y) and non-dispersive (horizontal, x) planes needed to be considered[1], a value for the offset had to be determined, which satisfied various requirements such as a momentum resolution, angular acceptance of e-beam and laser beam, and system compactness. The magnet center was placed such that the focusing strength in the dispersive plane provided sufficient momentum resolution, and that the slight defocusing in the un-dispersive plane kept the e-beam angular acceptance large enough. A vacuum chamber was designed to place the screen on the calculated first-order foci[24] for the bottom view. The forward view was designed to provide the maximum possible e-beam angular acceptance and reasonable system dimensions, as well as desired resolution for laser output mode measurements. A detailed evaluation of the resolution and acceptance are presented in the next section.

III. PERFORMANCE EVALUATION

The electron trajectories on the mid-plane (reference trajectories) were computed by calculating the deflection angle based on the Lorentz force. The input midplane field was generated through a 2D interpolation of the measured field profile along the radial axis. The representative trajectories (1.0, 0.5, 0.2, 0.1, 0.05, and 0.01 GeV) under a peak magnetic field $B_x(0) = 1.25$ T is shown in Fig. 1. Also shown is the magnetic field profile by color-map, and the locations of the screens. For each trajectory, the 6-dimensional e-beam properties were calculated by using the arbitrary order beam dynamics code COSY INFINITY (COSY)[25]. To utilize the most accurate fringe field evaluation in COSY, the magnetic field profiles for each trajectory were fitted into a six parameter Enge function $F(s)$ of the form

$$F(s) = \frac{1}{1 + \exp[a_1 + a_2(s/D) + \cdots + a_6(s/D)^5]}, \tag{1}$$

where s is the distance perpendicular to the effective field boundary, D is the gap of the magnet, and $a_1 - a_6$ are the Enge coefficients. In COSY, a particle trajectory $\boldsymbol{X(s)} =$

$(x, x', y, y', \delta l)$ is calculated in a form of fivefold Taylor expansion, where x (y) indicates horizontal (vertical) plane, $x' = dx/ds$, $y' = dy/ds$, and δl is the path length difference from the reference trajectory. For example, an expansion is written for x,

$$x = \sum (x|x_0^\kappa y_0^\lambda x_0^{'\mu} y_0^{'\nu} \hat{p}^\chi) x_0^\kappa y_0^\lambda x_0^{'\mu} y_0^{'\nu} \hat{p}^\chi. \tag{2}$$

Here, $\hat{p} = \delta p/p$ is a relative momentum spread, subscript 0 indicates that the quantity is evaluated at $s = 0$, namely at beam source, and $(x|x_0^\kappa y_0^\lambda x_0^{'\mu} y_0^{'\nu} \hat{p}^\chi)$ are the Taylor coefficients, which are function of s. The order is given by the sum $ord = \kappa + \lambda + \mu + \nu + \chi$. Shown in Fig. 2 are the spatial resolutions of the CCD cameras and each order's contribution to vertical size σ_{y1} versus e-beam energy (assuming zero energy spread), where σ is the root-mean-square (rms) width of the beam distribution, subscript 1 indicates the output (at the screens). The assumed peak magnetic field was 1.25 T, and the input beam profile was a Gaussian distribution with $\sigma_{x0} = \sigma_{y0} = 20$ μm, and $\sigma_{x'0} = \sigma_{y'0} = 2$ mrad (rms). The discontinuity at 160 MeV in Fig. 2 comes from the transition between different screens. One can see from Fig. 2 that the contribution from 3rd-order effects is small. Therefore, calculations up to 3rd-order give sufficient accuracy for the evaluation of the spectrometer performance. When the effective spatial resolution of the CCD camera is larger than the beam spot size, as in the low energy case, the momentum resolution would be limited by the CCD camera imaging (not the e-bam optics). Although the momentum resolution could be improved by an imaging system with higher spatial resolution, the scattering effect inside of the screens[21] has to be addressed for a beam size below a few 100 micron.

Due to the collimator-free scheme, the measured momentum resolution contained a contribution from the e-beam divergence, which depended on the accelerator configuration and parameters such as the laser energy or the capillary length and diameter. As the result, the e-beam divergence showed shot-by-shot fluctuation. Therefore, the momentum resolution and the energy spread were evaluated for each shot with the following procedure. From the computed imaging properties, the horizontal beam divergence $\sigma_{x'0}$ was calculated from the measured horizontal beam size σ_{x1} with a given beam size at the source, σ_{x0} and σ_{y0}, which were assumed to be the same size as the laser output mode size. The effect of the source size on the image was almost negligible since the beam size at the source was smaller by an order of magnitude than the typical product of beam divergence and propagation distance. By assuming an axisymmetric electron beam profile (i.e., equal horizontal and vertical

divergence), the vertical beam divergence $\sigma_{y'0} = \sigma_{x'0}$ was obtained and used to calculate the vertical beam size at the screen with a specific central energy and zero energy spread, σ_{y1mono}. The image size gave the intrinsic resolution of the ESM, δE_{mono}. The real energy spread of an electron beam δE_{beam} was then calculated by deconvolving the effect of finite divergence from the measured e-beam profile δE_{img} using $\delta E_{img} = \sqrt{\delta E_{beam}^2 + \delta E_{mono}^2}$. The momentum resolutions for $\sigma_{x'0} = \sigma_{y'0} = 1$ and 2 mrad electron beams are shown in Fig. 3, where the beam profile was assumed to be a Gaussian distribution with $\sigma_{x0} = \sigma_{y0} = 20$ μm. The momentum resolution is below 2% (4%) for 1 mrad (2 mrad) divergence beam in the energy range. As discussed, and shown in Fig. 2, in the case where the beam size is smaller than the spatial resolution of the CCD cameras, the momentum resolution is limited by the CCD camera resolution, which can be seen in the region where the 1 and 2 mrad cases overlap.

The collimator-free scheme also introduced an uncertainty in the determination of the absolute energy[15]. The energy of an electron beam with positive (negative) incident angle in y (see Fig. 1 for coordinates) would be measured higher (lower) than the actual energy. The errors in the determination of the energy of electrons with certain incident angle ($\pm$4 and $\pm$8 mrad) were computed and shown in Fig. 4, where the magnetic field was taken to be 1.25 T. For example, the electron beam measured as 1.0 GeV might have been 0.94 (1.07) GeV with a 0.4 (-0.4) mrad incident angle. The fluctuation level in the incident angle in the vertical plane was evaluated as follows. From the measured beam position in the horizontal plane x_{1peak}, the angular fluctuation in the horizontal plane σ_{x1peak} was statistically evaluated. With the assumption of symmetric behavior in both planes $\sigma_{y1peak} = \sigma_{x1peak}$, the fluctuations in the incident angle in the vertical plane was then determined. The angular fluctuations showed dependence on the accelerator configuration (e.g., the laser energy or the capillary length and diameter), and the typical value was found to be 2 to 6 mrad in rms[26], which gave $\sim \pm 3$ to 11% error at 1.0 GeV, or $\sim \pm 2$ to 5% error at 0.5 GeV. Also shown in Fig. 4 is the geometrical acceptance. The acceptance was trajectory dependent due to the differences in the path length and the imaging properties. More than $\pm$10 mrad acceptance was achieved in most of the energy range.

IV. EXPERIMENTS

In this section, we present examples of single-shot beam measurements and analysis. Experiments were performed by using a high peak power 10Hz Ti:sapphire laser system of the LOASIS facility at LBNL and gas-filled capillary discharge waveguides developed at Oxford University[14,15]. The laser beam was focused onto the entrance of a capillary discharge waveguide by an f/25 off-axis parabolic mirror. A typical focal spot size was $w \simeq 25$ μm, which gave a calculated peak intensity $I \simeq 2P/\pi r_s^2 \simeq 4 \times 10^{18}$ W/cm^2 and a normalized vector potential $a_0 \simeq 8.6 \times 10^{-10} \lambda[\mu\text{m}] I^{1/2}[\text{W/cm}^2] \simeq 1.4$ with full energy and optimum compression ($\simeq$ 40 fs, 40 TW).

Shown in Fig. 5 (a) is an example of a moderately resolved high energy e-beam. The capillary employed was 33 mm long, 220 μm diameter, on which a 37 fs, 41 TW laser was focused. The axial electron density[27] was $\simeq 4.3 \times 10^{18}$ cm^{-3}, and the applied magnetic field was 1.25 T. A mono-energetic beam with 778^{+39}_{-31} MeV peak energy and 10 pC total charge was observed. As stated in Sec. III, the estimated error range on the absolute energy value was computed from the beam angular fluctuation σ_{x1peak}, and found to be $\pm$0.38 mrad. The beam divergence was found to be $\pm$2.5 mrad (rms), which gave a resolution of 2.5% at 778 MeV. The energy spread was measured to be $\pm$4.6% (rms). Shown in Figs. 5 (b) and (c) are the examples of finely resolved mono-energetic and broadband e-beams, respectively. The 33 mm long, 190 μm diameter capillary was used with a 46 fs, 15 TW laser in Fig. 5 (b) and a 150 fs, 5 TW laser in Fig. 5 (c). The axial electron densities were $\simeq 3.4 \times 10^{18}$ cm^{-3}, and the applied magnetic field was 1.14 T, which gave momentum acceptances from 0.009 to 1.0 GeV. A discussion on the dependence of the CDG-LWFA performance on laser-plasma parameters is beyond the scope of this paper, and the details of the laser-plasma interaction are presented in Ref. 15. A mono-energetic beam with 364^{+9}_{-7} MeV peak energy and 10 pC total charge [Fig. 5 (b)] and a broadband e-beam (from 50 to 450 MeV) with 100 pC total charge [Fig. 5 (c)] were observed. For the mono-energetic beam [Fig. 5 (b)], the beam divergence was found to be $\pm$1.3 mrad (rms), which gave a resolution of 0.55% at 364 MeV. The energy spread was measured to be $\pm$5.0% (rms). For the broadband beam [Fig. 5 (c)], the divergence was $\simeq$ 2 mrad for the whole range, which gave less than 1% resolution as shown in Fig. 3. Note that the simultaneous diagnoses on laser output spots were successfully carried out for all measurements[14,15].

V. SUMMARY

A broadband slitless, single-shot electron spectrometer for GeV-class laser-plasma-based accelerator beam measurements has been developed at LOASIS facility of LBNL. A scint.-camera based system was employed for relativistic e-beam detection for high repetition rate experiments. The spectrometer covered from 0.01 to 1.1 GeV in a single shot, with the ability of simultaneous measurement of e-beam spectra and output laser properties due to the absence of a slit. The design provided an unprecedentedly large momentum acceptance of a factor 110 with reasonable resolution (below 5%). The design concept and hardware implementation were described, as well as the detailed analysis of the spectrometer performance. As shown in the Sec. IV, single shot measurements with sufficient resolution and angular acceptance were demonstrated. The spectrometer design provides a powerful diagnostic tool for the research and development of the next generation LWFA.

Acknowledgments

The authors acknowledge Gerry Dugan for contribution on the foci analysis, Bob Nagler and Michael Dickinson for implementation, Carl B. Schroeder, Anthony J. Gonsalves, Cameron G. R.Geddes, Csaba Toth, Eric Esarey for their contributions. K.N. acknowledges his faculty advisor Mitsuru Uesaka at University of Tokyo.

This work was supported by the U.S. Department of Energy under Contract No. DE-AC02-05CH11231.

* Also at Nuclear Professional School, University of Tokyo, Japan

[1] K. L. Brown, Tech. Rep. SLAC **75** (1975).

[2] T. Tajima and J. M. Dawson, Phys. Rev. Lett. **43**, 267 (1979).

[3] E. Esarey, P. Sprangle, J. Krall, and A. Ting, IEEE Trans. Plasma Sci. **24**, 252 (1996).

[4] A. Modena, Z. Najmudin, A. E. Dangor, C. E. Clayton, K. A. Marsh, C. Joshi, V. Malka, C. B. Darrow, C. Danson, D. Neely, and F. N. Walsh, Nature **377**, 606 (1995).

[5] C. A. Coverdale, C. B. Darrow, C. D. Decker, W. B. Mori, K.-C. Tzeng, K. A. Marsh, C. E. Clayton, and C. Joshi, Phys. Rev. Lett. **74**, 4659 (1995).

[6] D. Umstadter, S.-Y. Chen, A. Maksimchuk, G. Mourou, and R. Wagner, Science **273**, 472 (1996).

[7] C. I. Moore, A. Ting, K. Krushelnick, E. Esarey, R. F. Hubbard, B. Hafizi, H. R. Burris, C. Manka, and P. Sprangle, Phys. Rev. Lett. **79**, 3909 (1997).

[8] S. Mangles, C. Murphy, Z. Najmudin, A. Thomas, J. Collier, A. Dangor, E. Divali, P. Foster, J. Gallacher, C. Hooker, D. Jaroszynski, A. Langley, W. Mori, P. Norreys, F. Tsung, R. Viskup, B. Walton, and K. Krushelnick, Nature **431**, 535 (2004).

[9] C. G. R. Geddes, C. Tóth, J. van Tilborg, E. Esarey, C. B. Schroeder, D. Bruhwiler, C. Nieter, J. Cary, and W. P. Leemans, Nature **431**, 538 (2004).

[10] J. Faure, Y. Glinec, A. Pukhov, S. Kiselev, S. Gordienko, E. Lefebvre, J.-P. Rousseau, F. Burgy, and V. Malka, Nature **431**, 541 (2004).

[11] E. Miura, K. Koyama, S. Kato, N. Saito, M. Adachi, Y. Kawada, T. Nakamura, and M. Tanimoto, Appl. Phys. Lett. **86**, 251501 (2005).

[12] A. Yamazaki, H. Kotaki, I. Daito, M. Kando, S. V. Bulanov, T. Z. Esirkepov, S. Kondo, S. Kanazawa, T. Homma, K. Nakajima, Y. Oishi, T. Nayuki, T. Fujii, and K. Nemoto, Phys. Plasmas **12**, 093101 (2005).

[13] T. Hosokai, K. Kinoshita, T. Ohkubo, A. Maekawa, M. Uesaka, A. Zhidkov, A. Yamazaki, H. Kotaki, M. Kando, K. Nakajima, S. V. Bulanov, P. Tomassini, A. Giulietti, and D. Giulietti, Phys. Rev. E **73**, 036407 (2006).

[14] W. P. Leemans, B. Nagler, A. J. Gonsalves, C. Tóth, K. Nakamura, C. G. R. Geddes, E. Esarey, C. B. Schroeder, and S. M. Hooker, Nature Physics **2**, 696 (2006).

[15] K. Nakamura, B. Nagler, C. Tóth, C. G. R. Geddes, C. B. Schroeder, E. Esarey, W. P. Leemans, A. J. Gonsalves, and S. M. Hooker, Phys. Plasmas **14**, 056708 (2007).

[16] C. E. Clayton, M. J. Everett, A. Lal, D. Gordon, K. A. Marsh, and C. Joshi, Phys. Plasmas **1**, 1753 (1994).

[17] L. M. Chen, J. J. Park, K.-H. Hong, J. L. Kim, J. Zhang, and C. H. Nam, Phys. Rev. E **66**, 025402 (2002).

[18] C. Gahn, G. D. Tsakiris, K. J. Witte, P. Thirolf, and D. Habs, Rev. Sci. Instrum. **71**, 1642 (2000).

[19] H. Chen, P. K. Patel, D. F. Price, B. K. Young, P. T. Springer, R. Berry, R. Booth, C. Bruns, and D. Nelson, Rev. Sci. Instrum. **74**, 1551 (2003).

[20] K. A. Tanaka, T. Yabuuchi, T. Sato, R. Kodama, Y. Kitagawa, T. Takahashi, T. Ikeda, Y. Honda, and S. Okuda, Rev. Sci. Instrum. **76**, 013507 (2005).

[21] R.-I. I. Corp., Scintillator options for shad-o-box cameras, Technical Report AN-07, Rad-Icon Imaging Corp., www.rad-icon.com, Santa Clara, CA 95054, 2002.

[22] Y. Glinec, J. Faure, A. Guemnie-Tafo, V. Malka, H. Monard, J. P. Larbre, V. D. Waele, J. L. Marignier, and M. Mostafavi, Rev. Sci. Instrum. **77**, 103301 (2006).

[23] R. G. Schlecht and D. W. McColm, Phys. Rev. **142**, 11 (1966).

[24] G. Dugan, A. Misuri, and W. Leemans, Design and performance estimates for the l'oasis experiment magnetic spectrometers, Technical Report LBNL-49394, Lawrence Berkeley National Laboratory, University of California, Berkeley, CA 94720, 2001.

[25] K. Makino and M. Berz, Nucl. Instrum. Methods Phys. Res. A **427**, 338 (1999).

[26] K. Nakamura, E. Esarey, C. G. R. Geddes, A. J. Gonsalves, W. P. Leemans, D. Panasenko, C. B. Schroeder, and C. Toth, in *Proceedings of the 2007 Particle Accelerator Conference*, p. 2978, Piscataway, NJ, 2007, IEEE.

[27] A. J. Gonsalves, T. P. Rowlands-Rees, B. H. P. Broks, J. J. A. M. van der Mullen, and S. M. Hooker, Phys. Rev. Lett. **98**, 025002 (2007).

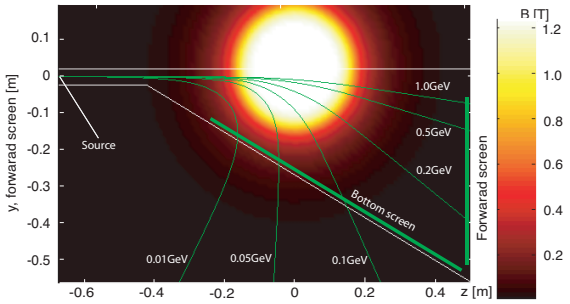

FIG. 1: (Color) Electron trajectories (1.0, 0.5, 0.2, 0.1, 0.05 and 0.01 GeV) with a peak magnetic field of 1.25 T. The location of the phosphor screens and the vacuum chamber are also illustrated. The center of the magnet is at $z = 0$. Shown by color-map is the magnetic field profile. The source is the exit of the capillary discharge waveguide.

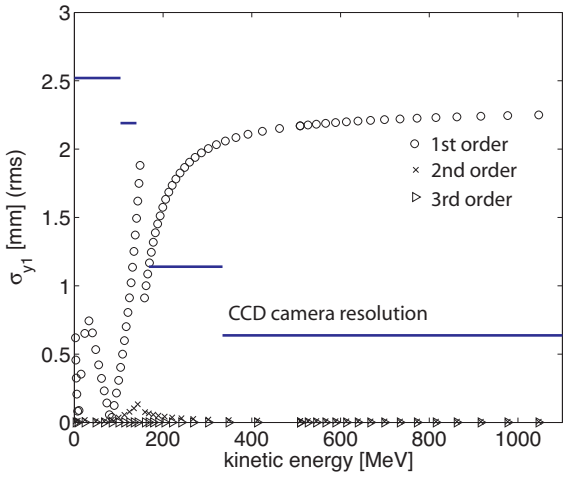

FIG. 2: (Color online) Calculated contributions to the vertical beam size of each order. Assumed input beam profile is Gaussian distribution with $\sigma_{x0} = \sigma_{y0} = 20$ μm (rms), and $\sigma_{x'0} = \sigma_{y'0} = 2$ mrad (rms). Horizontal axis is the kinetic energy of electron for the peak magnetic field of 1.25 T. Also shown is spatial resolution of CCD cameras.

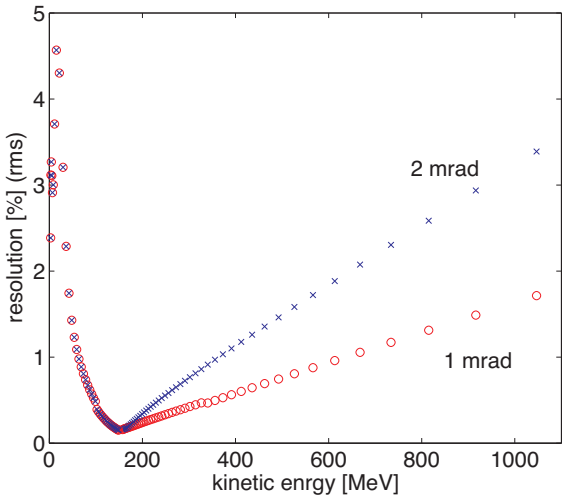

FIG. 3: (Color online) Momentum resolutions for $\sigma_{x'0} = \sigma_{y'0} = 1$ and 2 mrad electron beams. Horizontal axis is the kinetic energy of the e-beam for the peak magnetic field of 1.25 T. The input beam size was assumed to be a Gaussian distribution with $\sigma_{x0} = \sigma_{y0} = 20$ μm.

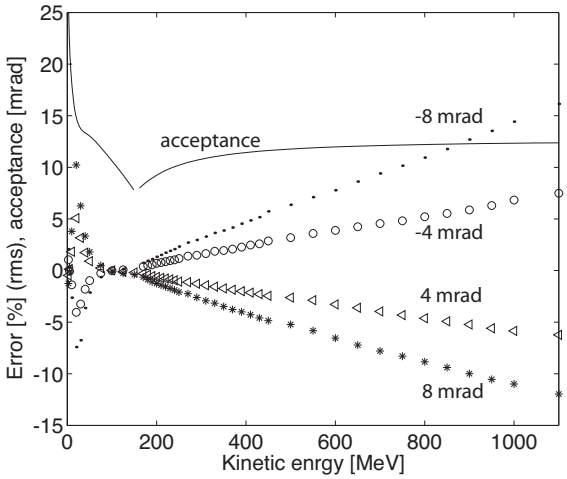

FIG. 4: Errors in the determination of the absolute energy in cases of ± 4 and ± 8 mrad of the incident angle with the geometrical acceptance. The magnetic field was assumed to be 1.25 T.

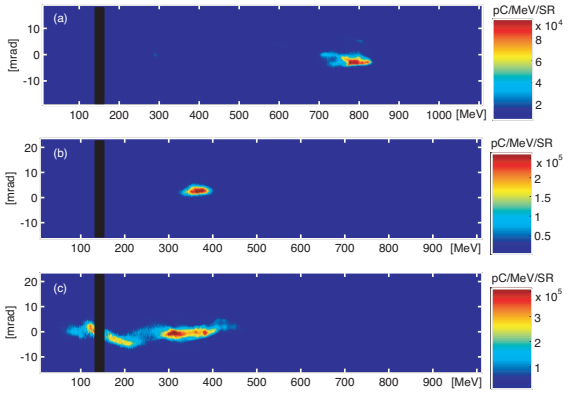

FIG. 5: (Color) Single shot spectra: (a) moderately resolved high energy e-beam, (b) finely resolved mono-energetic beam, and (c) finely resolved broadband beam.